Scales and processes in the aggregation of diatom blooms: high time resolution and wide size range records in a mesocosm study

L. Prieto[a,*], J. Ruiz[b], F. Echevarría[a], C.M. García[a], A. Bartual[a], J.A. Gálvez[a], A. Corzo[a], D. Macías[a]

[a] *Área de Ecología, Facultad de Ciencias del Mar, Universidad de Cádiz, 11510 - Puerto Real, Cádiz, Spain*
[b] *Instituto de Ciencias Marinas de Andalucía (CSIC), Avenida de la República Saharaui, S/N, 11510 - Puerto Real, Cádiz, Spain*

Abstract

Diatoms and the large, fast-sinking aggregates they form during blooms play an important role in downward flux of particles in the ocean. To study how the aggregation process operates on particle dynamics, diatom blooms were generated and followed under controlled conditions in nutrient-enriched laboratory mesocosm where a homogeneous mixed surface layer was emulated. The size spectrum of particles (from 12 μm to several mm) was recorded each hour during the 1 month span of the experiment by a non-intrusive image analysis system with two CCD cameras. Beam attenuation was continuously recorded as an additional estimator for particle abundance. The high time resolution and wide size range of the records obtained with this design were able to resolve the time scale for coagulation as well as to determine the lowest time resolution needed to sample any experiment aimed to study aggregation of diatoms. Our results narrow previous theoretical time scales to the order of hours to days for the process of mass transfer from small particles to marine snow. Also, daily analyses of a broad range of biological and chemical variables permitted to link phytoplankton succession to the aggregation process. Finally, the evaluated role of different copious exopolymers suggested a lower implication of Coomassie stained particles (CSP) than transparent exopolymeric particles (TEP) in the formation of marine aggregates. © 2002 Published by Elsevier Science Ltd.

Keywords: Aggregation; Diatoms; Particle size; Image processing; TEP; CSP

1. Introduction

Diatom blooms represent singular situations to the pelagic ecosystem, as both energy and matter trophic transfers are out of balance because of the decoupling between primary and secondary production. A large fraction of the subsequent excess of primary production terminates by the massive aggregation of cells, which rapidly settle out of the

*Corresponding author. Marine Biology Division, Lamont-Doherty Earth Observatory, Columbia University, PO Box 1000, Palisades, NY 10964, USA. Tel.: +1-845-385-8449; fax: +1-845-365-8150.

E-mail address: pgalvez@ldeo.columbia.edu (L. Prieto).

sea surface as large, fast-sinking particles (Alldredge and Gotschalk, 1989; Riebesell, 1991a, b; Kiørboe et al., 1994; Scharek et al., 1999). This makes diatoms and their aggregates an important component in the transfer of oceanic carbon from the surface to the deep ocean (Fowler and Knauer, 1986; Alldredge and Gotschalk, 1989; Jackson and Lochmann, 1992).

Since field data provide evidence for the importance of physical (of abiotic nature, coagulation, hereafter) versus biological (mediated by zooplankton) aggregation mechanisms to explain high postbloom vertical fluxes (cf. Smetacek, 1985), the coagulation process has stimulated theoretical and empirical research. Aggregation theory applied to the marine environment emphasizes that particle size is a key variable to record in any experiment aimed at analyzing the process of coagulation (McCave, 1984). This imposes a difficulty, since marine flocs resulting from coagulation, although stable in the water, are fragile when manipulated, and their sizes can be adequately measured only by non-intrusive techniques (Eisma et al., 1996). Another relevant aspect of coagulation is how rapid the material is drafted to large particles and consequently lost from the upper ocean, since this marks their potential remineralization before sinking out of the mixed layer. Although theory gives estimated time scales for the process of coagulation ranging from minutes to more than a week (Jackson, 1990; Riebesell and Wolf-Gladrow, 1992; Hill and Nowell, 1995), experimental data recorded at high time resolution is still required to verify those time scales.

One of the elements with highest potential to reduce the time scale of coagulation is the extracellular polymeric material secreted by pelagic phytoplankton. These exudates enhance the attachment probability by acting as a biological glue, which makes particles stay together once inter-particle contact has occurred. They are known as transparent exopolymeric particles (TEP) (Alldredge et al., 1993) and are generated abiotically from polysaccharide precursors released mainly from diatoms as dissolved and colloidal matter (Chin et al., 1998; Zhou et al., 1998; Passow, 2000). More recently, Long and Azam (1996) found other particles, the Coomassie

stained particles (CSP), whose abundance in the marine ecosystem is similar to that of TEP and thus potentially as important for coagulation. CSP consist of proteins, which also form polymers, and their role in the coagulation of particulate matter has not been previously investigated.

Regarding both mechanisms and particles involved in coagulation, the SIGMA tank experiment (Alldredge and Jackson, 1995) represented a remarkable step in understanding this process. The modulation of particle stickiness by TEP (Dam and Drapeau, 1995), the role of phytoplankton-bacteria association in TEP formation (Smith et al., 1995), the structure of the community in the formation of aggregates (Alldredge et al., 1995) and the ability of coagulation theory to reproduce changes in particle size spectra due to coagulation (Jackson, 1995) were explored in this experiment. The SIGMA experiment displayed the potential of mesocosms for investigation of coagulation and identified important issues on the time scale, the size of particles involved, and the time resolution needed in future research on phytoplankton coagulation.

This information was incorporated in the design of the mesocosm experiment presented in this paper, which represents an experimental simulation of a homogeneous mixed surface layer where coagulation of diatom blooms is occurring. The use of automation and two CCD cameras allowed the recording of the size structure of particles in a wide size range (from 12 μm to several mm) at very high time resolution (1 h) for a period longer than a month. This design was able to resolve the time scale (of the order of hours to days) associated with the mass transfer from small to large particles of marine snow. In addition, the experiment incorporated the continuous record of light beam attenuation as well as daily analysis of a broad range of biological and chemical variables relevant to the aggregation process. This information allowed tracking of the role of the abundance and size dynamics of TEP and CSP, bacteria and algal biomass (from pico to microplankton), particulate organic matter, phytoplankton species and nutrient concentrations in the intensity and velocity at which coagulation occurred in a twice blooming system.

2. Material and methods

2.1. Experimental design

An octagonal glass mesocosm 0.6 m high and 1 m^2 was filled with 455 l of 0.2 μm-filtered seawater from the Bay of Cádiz (southern Spain). On Day 0 (July 9, 1998), 20 l of unfiltered surface seawater from this bay were added to the mesocosm as an inoculum. In addition, inorganic nutrients were added with an initial concentration of 63 μM nitrate, 32 μM silicate and 1.7 μM phosphate. Trace metals (Cl$_3$Fe, 0.42 μM; SO$_4$Cu, 0.32 μM; SO$_4$Zn, 0.70 μM; Cl$_2$Co, 0.32 μM; Cl$_2$Mn, 5.76 μM; MoO$_4$Na, 0.20 μM) and vitamins (B12, 0.36 μg l^{-1}; Thyamin, 7.12 μg l^{-1}) were also added.

Artificial light was provided by eight fluorescent lamps set at 30 cm above the water surface, with a light intensity of 125 ± 19 μE m^{-2} s^{-1} at 15 cm from the lamps. During the 37-day span of the experiment the temperature of the water in the mesocosm was relatively constant ($27.1 \pm 0.7°$C).

2.2. Physical environment

Turbulent flow was generated to create spatial homogeneity, especially along the vertical axis, since the mesocosm simulates a 0-D process and sedimentation generates vertical structure (Ruiz, 1996). It was important to avoid any interference with the aggregate imaging system. Turbulent flow was generated by a design akin to a Couette flocculator (Fig. 1A): Reynolds Number $= \omega \Gamma L / \eta > 3$ E5, where ω is the angular velocity, Γ is the radius of the rotating cylinder, L is the distance between the inner cylinder and aquarium wall and η is the kinematic viscosity. A flat ruler at the bottom of the inner rotating axis, generated strong very local turbulence at the bottom of the mesocosm to avoid particle trapping at the floor. The radius of the rotating cylinder was 5 cm. An estimation of the dissipation of turbulent energy (ε) in the mesocosm was determined on dimensional grounds by considering a spatial scale ($L = 50$ cm) and calculating the fluctuating part of the velocity (u')

$$\varepsilon \approx \frac{(u')^3}{L} \quad \text{(Tennekes and Lumley, 1972)}$$

u' was estimated with the imaging system described below by computing instantaneous particle displacements between successive images (Tennekes and Lumley, 1972). This fluctuating velocity was estimated at 23 cm from the inner cylinder, approximately equidistant from the cylinder and the mesocosm wall. The two velocity directions that could be computed with our focal plane imaging technique (tangential u' and vertical w') resulted in a value of 0.48 cm s^{-1} ($n = 525$ in both cases). This produces an of the order of 10^{-7} m^2 s^{-3} for the mesocosm, a value typical of those found in surface mixed layer waters. An estimation for eddy diffusivity (n_t) in the mesocosm can also be computed on dimensional grounds, $n_t = Lu'$, resulting in values of the order of 10^{-3} m^2 s^{-1}. On the basis of dimensionless diffusivities of particles (Ruiz, 1996) this implies that particles with a settling velocity less than about 400 m d^{-1} are homogeneously distributed in the aquarium. This high velocity embraces all particles produced during the experiment.

2.3. Aggregate abundance

The abundance and size distribution of aggregates in the mesocosm were obtained from non-intrusive images of particles generated by two COHU$^®$ CCD cameras (Fig. 1B). These cameras focused on the interior of the mesocosm at a point 30 cm from the inner cylinder and 30 cm above the bottom. One camera was mounted on a microscope (Leica Wild M10) and sampled particles from 9 to about 200 μm of ESD (equivalent spherical diameter). The other camera was mounted on a macro objective (Nikon AF Micro Nikkor) and was able to sample particles from about 80 μm to millimeters of ESD. Both registers were combined after the experiment to obtain the whole particle size spectrum from micro to centimeters (Fig. 2). Camera shutter speeds were set to provide a 1/250 s exposure time.

A laser (56DLB272/p1, Melles Griot) and a halogen light (Oriel, QTH 100 W), orthogonal to the cameras, produced two collimated slabs of light in which particles were highly illuminated. Collimation is required to get a well-defined light beam, which allows the dimensions of the slab of
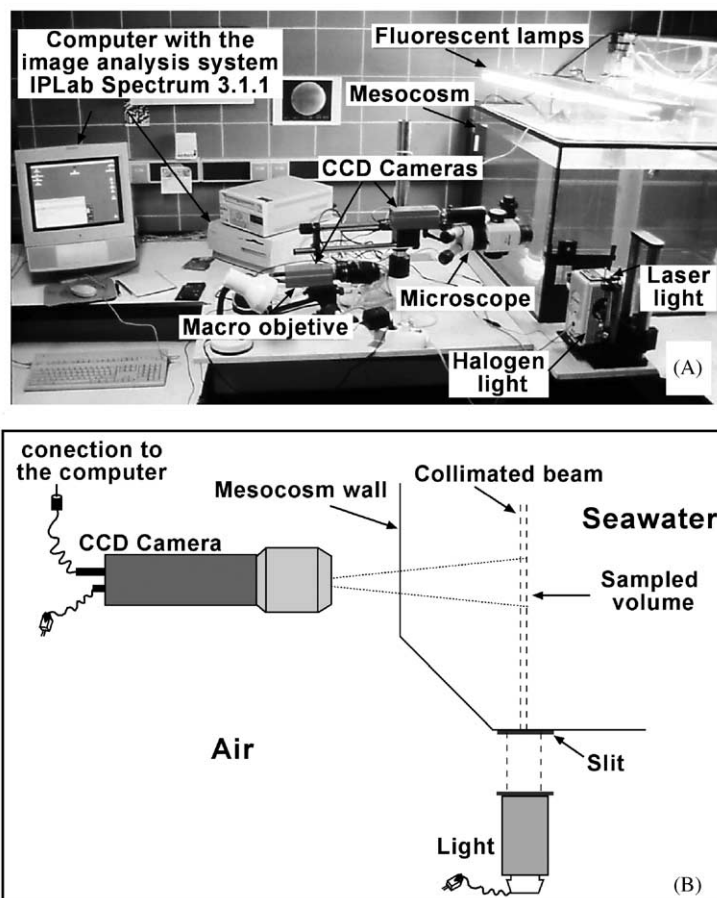
Fig. 1. Experimental design. (A) Entire mesocosm and image analysis system (IAS). The photograph shows a previous mesocosm design, which was square instead of octagonal. (B) Close-up diagram of one camera and the light configuration.

water sampled to be known. The thickness of each beam was set by passing the lights through slits (580 μm and 1 cm for laser and halogen lights, respectively). A thin beam of light was used to prevent sizing errors resulting from out-of-focus particles. The microscope camera sampled a slab of seawater of 2310 μm (height) × 3460 μm (width) × 580 μm (depth) size and 4.64 μl volume, and the macro camera sampled a slab of seawater of 2.31 cm × 3.46 cm × 1 cm size and 8 ml volume.

Cameras were linked to a Macintosh computer through a digitizer board (LG-3 Scion Corporation®) provided with the image analysis software IPLab Spectrum 3.1.1 (Signal Analytics Corpora-

tion®). One image is an array of 768 × 512 pixels where each pixel has a gray-level between 0 (black) and 255 (white). Particles are defined as a connected region of pixels with a gray-level higher than a threshold. The software distinguishes background pixels from pixels identified as particles by creating an overlay where those pixels are selected. Further processing, involving dilating and eroding, is performed on the overlay in order to improve particle outlines before the automated count/measure facility is used to size the particles in the original image.

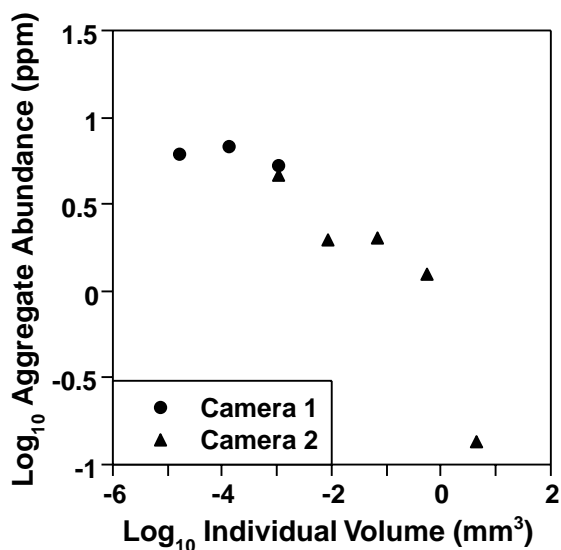The relative size of 1 pixel is computed for each camera with a graduated slide positioned within

Fig. 2. An example of particle size distributions of the two camera systems. "Camera 1" and "Camera 2" refer to the one mounted on the microscope and on the macro objective, respectively. The overlap of the two registers is in the 80–160 μm spherical equivalent diameter (ESD) size class.

the focus field (1 pixel = 4.5 and 45 μm for microscope and macro camera, respectively). We employed homogeneous suspensions of materials whose composition, size, and optical properties were variable, including pollen, ground coffee particles, and several phytoplankton cultures, to calibrate the image analysis system (IAS). The concentration and sizes of those materials were determined under an inverted microscope according to Utermöhl (1958) with a video-interactive image analyzer described later. There was a good correspondence between estimated particle sizes obtained with inverted microscope and IAS techniques although deviations were detected in the concentration during the first calibration experiments. These differences were caused by a halo that appeared around the light beam when in the mesocosm as a result of the interaction of light with water or small particles. Some particles might be affected by the halo and acquire a gray-level too close to the background gray-level. We corrected for this effect by calculating the depth of the halo (h_z) after assuming that it is independent of the slit

width (z) and implementing several of these slits. The sampled volume is: $V = x \cdot y \cdot (z + h_z)$, where x is the width and y is the height. The concentration (C_r) is estimated by: $C_r = N_{\text{nom}}/V$, where N_{nom} is the number of recorded particles. Then, with two different slits (1 and 2)

$$C_{r1} = \frac{N_{\text{nom1}}}{xy(z_1 + h_z)} \quad \text{and} \quad C_{r2} = \frac{N_{\text{nom2}}}{xy(z_2 + h_z)} \qquad (1)$$

and if $C_{r1} = C_{r2}$, then

$$h_z = \frac{N_{\text{nom2}}z_1 - N_{\text{nom1}}z_2}{N_{\text{nom1}} - N_{\text{nom2}}}. \qquad (2)$$

We conducted experiments to find the required settings (digitization limits to capture the image) that minimize h_z but include all the particles that are correctly illuminated within the slab of light. With the implemented setting, h_z was negligible for both laser (0 ± 1 pixels) and halogen (0 ± 4 pixels) lights, and a good correspondence was obtained between inverted microscope and IAS techniques to estimate particle concentration.

As particles with dimensions smaller than the pixel size of the CCD-camera can still be observed if enough light is reflected, we rejected particles smaller than three interconnected pixels in one direction. That occurred when the particle was at least 5 pixels (that is when all the possible combinations of particles with 3 pixels in one direction are considered), so the size of the smallest particle to be detected was determined as 11.3 μm of ESD, corresponding to a particle of 5 pixels registered with the microscope camera. The following data were taken for each particle image of at least 5 pixels: area, perimeter, major and minor axis, an index of shape, the position, and the mean and average gray tone value (reflectivity). Particle volume (equivalent spherical volume, ESV) was estimated from the measured particle area, assuming that equivalent circular diameter is the same as the ESD of the particle. This is the most accurate estimation of particle volume when focal plane techniques are used (Stemman, 1998). Particle volume concentrations, expressed as the volume of particles per volume of water in parts per million (ppm), were determined from the ESV of the particles. Data were arranged into size classes of ESD whose amplitude is equal to the

lower limit of that class. The first size class was 20–40 μm of ESD and the last 640–1280 μm.

The computer was programmed to sample the mesocosm each hour during the 37-day span of the experiment. At the sampling time, the computer recorded 1000 images with the microscope camera and 30 images with the macro camera. The system produced high contrast bright field exposures and obtained one image each 0.2 and 0.8 s for the microscope and macro camera, respectively. A previous assay of different elapsed times showed that these frequencies ensured that the successive images were independent. The total volume sampled after summing the individual volumes of the 1000 and 30 images, respectively, was 4 and 250 ml. The number of images recorded from each camera was set to sample a total volume in accordance with particle densities of natural systems (Riebesell, 1991a; Kepkay et al., 1993; Lampitt et al., 1993) and mesocosm studies (Alldredge et al., 1995). It is also a compromise between maximizing temporal resolution and statistical strength of the resulting data. Light over the mesocosm was switched off during the time required to record the images.

2.4. Biological and chemical analyses

In addition to a detailed record of particle dynamics, several biological and chemical variables were studied. Temperature and beam attenuation were continuously registered during the experiment. Beam attenuation was measured with a C-STAR transmissometer (Wet-Labs, Inc.) working with a 660 nm beam of light and 25 cm of path length. Daily values of photosynthetically active radiation (PAR) were also recorded, with a LI-193 SA Spherical Quantum Sensor (LiCor, Inc.) under the water surface.

Discrete samples for further analyses were collected twice a day, once a day or every 2 days depending on the stage of the bloom. Samples were taken through a glass tube (inner diameter: 1.5 cm) that drew water ≈ 30 cm from the mesocosm wall and 26 cm off the bottom. Triplicate samples for nutrients were filtered through Whatman GF/F glass fiber filters and stored in polypropylene bottles at $-30°C$ until analysis of

nitrate, nitrite, ammonium, silicate and phosphate with an autoanalyser TRAACS 800. Extracted chlorophyll *a* (chl *a*) and phaeopigments were measured on 3–5 replicates of 50–200 ml samples by standard fluorometric methods (Parsons et al., 1984) with a Turner Designs Model 10 fluorometer. Total particulate organic carbon (POC) and nitrogen were determined on triplicate samples of 100–500 ml each collected on precombusted 25 mm Whatman GF/F glass fiber filters and analyzed on a Perkin-Elmer 240-C analyzer, according to JGOFS protocols (Unesco, 1994).

Samples of 3 ml for flow cytometric analysis were preserved in triplicate in cryogenic tubes with a final concentration of 1% glutaraldehyde. Samples were frozen in liquid nitrogen and stored until analysis (Vaulot et al., 1989) with a flow cytometer Becton Dickinson Model Fac-Scalibur. Only the fraction of cells discriminated by the large size (measured by "forward scatter") and the red fluorescence was used.

Bulk samples for bacterioplankton enumeration were preserved in 0.6% glutaraldehyde and stored in the dark at 4°C until analysis. Triplicate subsamples 1–4 ml were stained in the dark for 10 min with 4′,6-diadimino-2-phenylindole (DAPI; 1 μg ml^{-1} final). Each subsample was then filtered onto 0.2 μm pore-sized black polycarbonate filters (Poretics), mounted in immersion oil on a microscope slide and a coverslip added (Porter and Feig, 1980). The slide was examined at 1000 × with a Leitz Laborlux epifluorescent microscope.

For plankton enumeration, samples of 125 ml were preserved with acetic Lugol for microscope analysis. The plankton size structure was analyzed by the inverted microscope method of Utermöhl (1958). Cells were counted at 200 × and 400 × on a Leitz Fluovert microscope assisted by a VIDS-V (Analytical Measuring System) video-interactive image analyzer. Each organism was assigned to a taxonomic category, being considered as "phytoplankton" that autotrophic fraction of the total and "plankton" the summary of all counts. Biovolume for each individual organism was estimated by assigning a certain geometric shape to the individual. By using this technique we were able to study plankton in a size range from 2 to 80 μm of equivalent spherical diameter (ESD). The

size measurements obtained were grouped into classes arranged in octaves (2^n) of the individual volume. Nominal volumes (v) of size classes have been defined as $v = 1.44w$, w being the lower limit of the size class (Blanco et al., 1994). The techniques of Platt and Denman (1977, 1978) were used to fit a linear function to the log-transformed normalized volume. The slope (b) can be used to assess the size characteristics of the plankton community. Larger values of b correspond to a greater proportion of small cells. Diatoms were identified with a JEOL-820 scanning electron microscope (SEM) with Robinson et al. (1987) protocols.

Bulk samples were preserved in 1% 0.2 μm filtered formalin for colorimetric determination of TEP concentration (Passow and Alldredge, 1995). Formalin does not interfere with the staining procedure itself (Passow and Alldredge, 1994; Schuster and Herndl, 1995). Six replicate 25–150 ml subsamples were filtered onto 0.4 μm pore-size polycarbonate filters (Poretics), then TEP was stained with an Alcian Blue solution and the dye redissolved in sulfuric acid. Gum Xanthan was used to calibrate the dye and results are expressed as μg l^{-1} Gum Xanthan equivalent (μg Xeq. l^{-1}). For the microscopic observation of TEP and CSP abundance samples were collected and processed within 1 h. For CSP particles the method of Long and Azam (1996) was used. For TEP the method of Alldredge et al. (1993) as modified by Logan et al. (1994) was followed. Blanks for both CSP and TEP staining methods were done every day. All the slides were examined immediately by light microscopy at 250 × magnification. 400 particles were sized and enumerated per filter using the same IAS used for plankton. The size measurements were grouped into increasing size classes and the normalized size spectra obtained by the same methodology as described for plankton. Size spectra of TEP and CSP were done separately with at least five size classes unambiguously covered.

Five liters of filtered seawater (with same nutrients concentrations as in the initial inoculum) were added to the mesocosm (representing 1% of the total enclosure volume) to compensate for the volume removed by sampling. The added water did not show any effect on the continuous registers of concentration of particles by either transmissometer or IAS.

3. Results

Two blooms of diatoms were observed in the mesocosm: the first bloom peaked on Day 14 after inoculation and the second on Day 21 (Fig. 3). The general progress of the blooms, as indicated by biological and chemical variables, followed a pattern of succession discussed in detail below. A pre-bloom period, characterized by low values of chl *a*, was observed the first week of the experiment. It was followed by an exponential increase of phytoplankton until a rapid decrease occurred days 15–16 accompanied by a taxonomic change in the community, which led to a second bloom. The decay of this new bloom was associated with nutrient depletion after Day 22.

3.1. Nutrient availability, plankton abundance and species composition

During the pre-bloom period a progressive decline of nitrate and soluble reactive phosphorus (SRP) was observed, and the concentration of chl *a* increased by a factor of five although this is not easily seen in Fig. 3. The local maximum of POC and particulate nitrogen (PN) observed on Day 4 was not related to autotrophic organisms as it was not recorded in the values of chl *a* or ultraplankton abundance.

Chl *a* reached a concentration of 40 μg l^{-1} during the second bloom compared to the preceding 15 μg l^{-1} (Fig. 3A). Inorganic nutrient concentrations showed a depletion pattern related to the development of phytoplankton blooms. SRP remained low after the first bloom (Day 15) with most values observed around 0.03 μM (Fig. 3B). Nitrate and silicate, on the other hand, reached low concentrations only after the second bloom (Figs. 3A and B). The concentrations of ammonium and nitrite followed a different pattern, probably related more to microbial processes in the mesocosm. The pattern of variation of phytoplankton biomass was reflected by changes
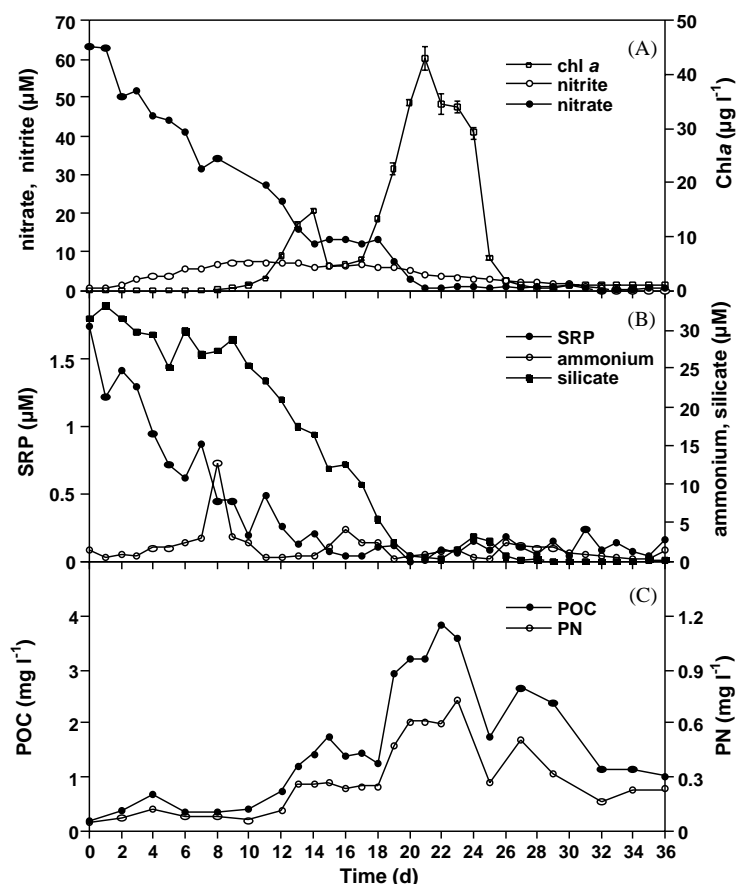
Fig. 3. Nutrients (μM), chl *a* (μg l^{-1}) and particulate organic matter (mg l^{-1}) concentrations during the study. (A) Nitrate, nitrite and chl *a*. Bars represent standard deviation ($\pm$ SD, $n > 3$). (B) Soluble reactive phosphorus (SRP), silicate and ammonium. (C) Particulate organic carbon (POC), filled circles, and particulate nitrogen (PN), empty circles.

in POC and PN (Fig. 3C). POC and PN reached maxima the day after each bloom peaked. Carbon to nitrogen ratio did not show any tendency throughout the study (average 6.5 ± 1.1).

A community of non-chain-forming diatoms, especially *Nitzschia closterium* and *Thalassiosira oceanica*, dominated the first bloom. *Skeletonema costatum*, various species of small naked nano-flagellates and one unidentified Prymnesiophyta were also present (Fig. 4). Cell aggregates, primarily consisting of *N. closterium* and *T. oceanica*, were formed after Day 12. The composition of these aggregates was further examined by SEM (Fig. 5A), and living diatoms made up most of

material in the aggregates. The second bloom was dominated by the chain-forming diatom *S. costatum*, which also formed aggregates together with *T. oceanica* and other diatoms (Fig. 5B). But aggregates were less dense than those generated after the first bloom, as was observed by light microscopy and by lower values of average particle reflectivity registered by IAS. Plankton abundance increased from 8000 cells ml^{-1} on Day 8 to 115,000 cells ml^{-1} on Day 14 (first bloom) and to more than 160,000 cells ml^{-1} on Days 18 and 21 (second bloom; Fig. 4A). Plankton biomass, expressed as biovolume (mm^3) per liter, increased from 0.07 mm^3 l^{-1} initially concentrations to 4 and
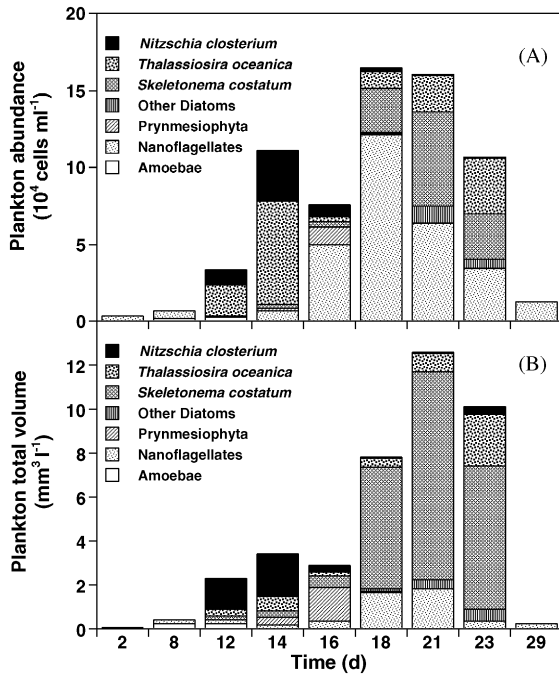
Fig. 4. Composition of the plankton community over the course of the study as estimated by a video-interactive image analyzer. (A) Cell abundance (10^4 cells ml^{-1}) and (B) total plankton biovolume (mm^3 l^{-1}).
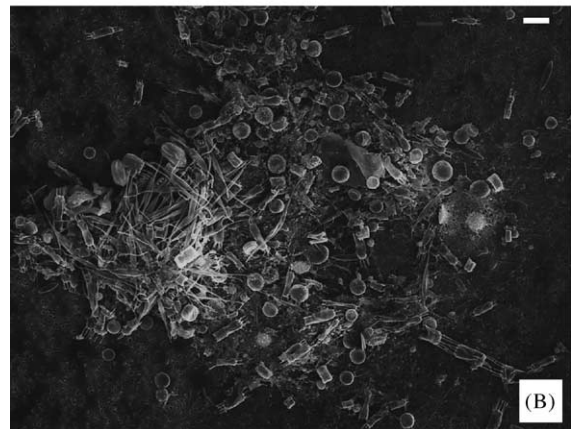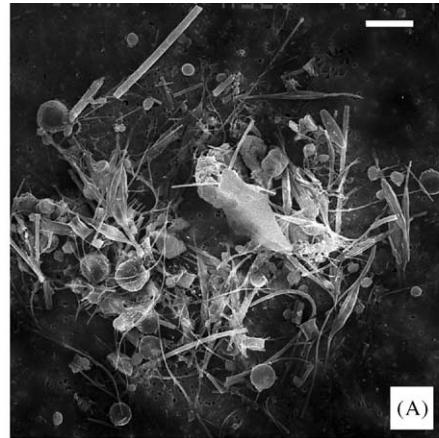

Fig. 5. Scanning electron microscopy (SEM) micrographs of aggregates. (A) Aggregate of the first bloom and (B) aggregate of the second bloom. Both scale bars are 10 μm long.

12 mm^3 l^{-1} during the first and second bloom, respectively (Fig. 4B).

Cell abundance of phytoplankton measured by flow cytometry (Fig. 6A) and of the autotrophic fraction measured by microscopy, were very similar ($r^2 = 0.91$). This similarity is due to the fact that the dominant diatoms of both blooms were small (from 3 μm of ESD of *T. oceanica* to 6 μm of ESD of *N. closterium* and the 11 μm of ESD of *S. costatum*). Therefore, all dominating diatoms were inside the size range covered by flow cytometry, although some *N. closterium*, with its elongated shape, probably fall out of that size range.

Phytoplankton size distributions changed during the experiment, shifting toward larger sizes as reflected by a decrease of size spectrum slopes (Fig. 7). *S. costatum* colonies increased the average diameter together with the average colony length (Fig. 8C) during the second bloom. In the first bloom, *T. oceanica* increased the average diameter

(Fig. 8B), although average length of *N. closterium* slightly decreased although not significantly (Fig. 8A).

Bacteria increased from 0.6×10^6 ml^{-1} (Day 0) to 10.8×10^6 ml^{-1} (Day 21, Fig. 6B). Thereafter, the bacterial abundance fluctuated around 8×10^6 ml^{-1}, with the maximum on Day 19 and a minimum on Day 23. Two clear bacterial populations could be distinguished (Fig. 9). At the beginning of the study, coccoid-shaped bacteria (Fig. 9A) were the most abundant, coexisting with a population of much larger and filamentous bacteria (Fig. 9B). These larger bacteria were predominant at the end of the study.
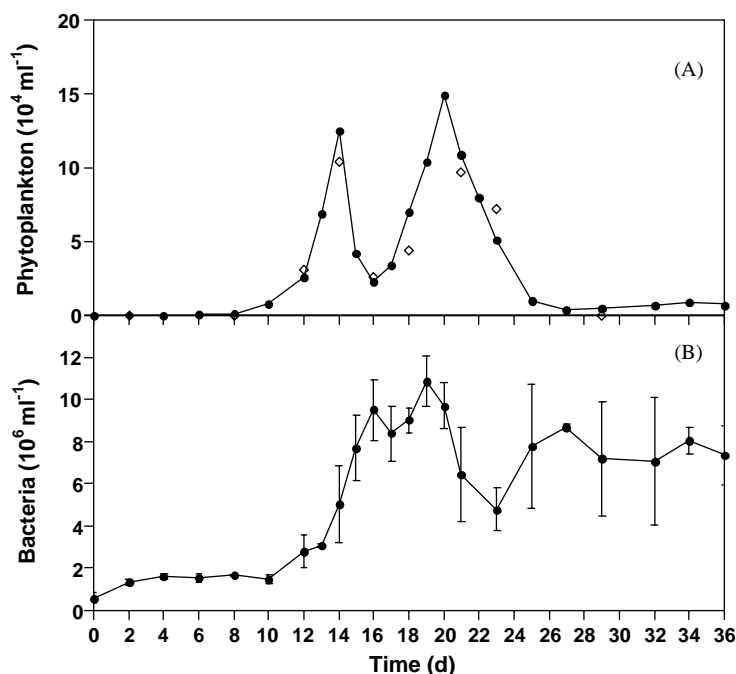
Fig. 6. Phytoplankton and bacteria over the course of the experiment. (A) Phytoplankton cell abundance measured by flow cytometry (filled circles) and by light microscopy (empty diamonds). A good correspondence between the two measurements can be observed. (B) Bacterial abundance measured by epifluorescence microscopy. Bars represent standard deviation ($\pm$SD, $n = 3$).

3.2. Aggregate abundance and size distribution

The hourly particle size spectra in the mesocosm obtained with the IAS (Fig. 10) show that particle concentration maxima were visible just after the peak of the blooms, from Day 14 to 18 and from Day 23 to 26. Also, a small peak was observed around Day 5, which was related to the non-autotrophic pulse of mass. The particle maximum associated with the first bloom was composed of aggregates larger than those of the second bloom, whereas the aggregate abundance was smaller.

A comparison between size spectra obtained with IAS and those obtained from the more conventional light microscopy is not straightforward. Each method covered a different size range, and even though the video-interactive image of light microscopy could study particles up to 80 μm of ESD, the plankton, TEP and CSP observed by this method were smaller. Plankton maximum size (observed on Day 23) was close to 20 μm ESD, and

the biggest TEP and CSP were around 28 μm ESD, whereas the first size class considered well covered by the IAS was 20–40 μm. Nevertheless, the data from both methods were compared in terms of average particle size (expressed as volume). The size ratios of TEP and CSP (measured by microscopy) to aggregates (all particles measured by IAS) were not significantly different between the two types of exopolymers or between the two aggregate maxima (Table 1). We consider as *aggregates* the particles measured by the IAS (from 20 to 1280 μm), since the lower cut-off implies that they are particles formed by collision of two smaller particles, as the primary (not formed by collision) particles in this study were smaller than 20 μm. The size ratio of plankton to aggregates was slightly higher during the second bloom compared to the first (probably related to larger size of *S. costatum*).

Plots of the total particle concentration measured with the IAS (Fig. 11B) and the beam attenuation values measured with the transmis-
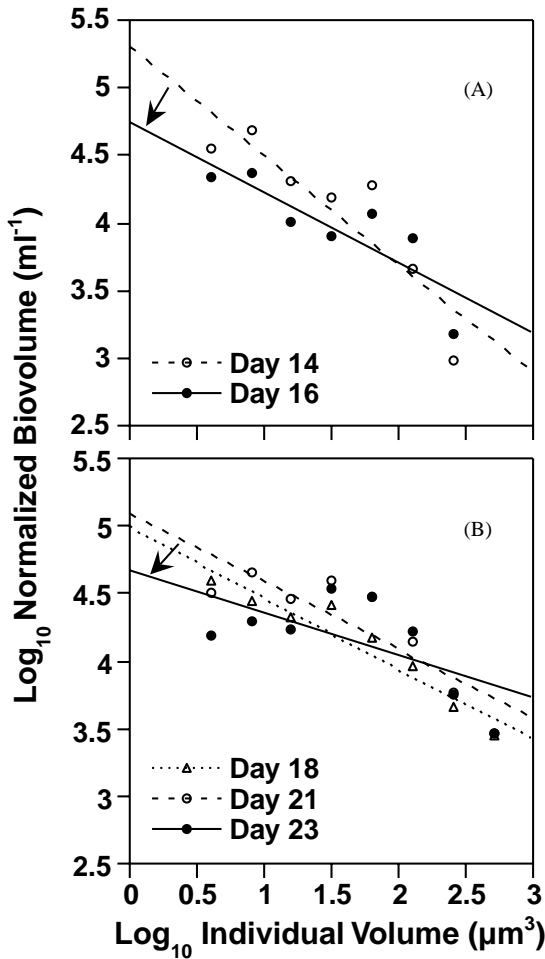
Fig. 7. Time evolution of normalized biomass size spectra of phytoplankton from daily samples. (A) During and after the first bloom (Days 14 and 16) and (B) before, during and after the second bloom (Days 18, 21 and 23).
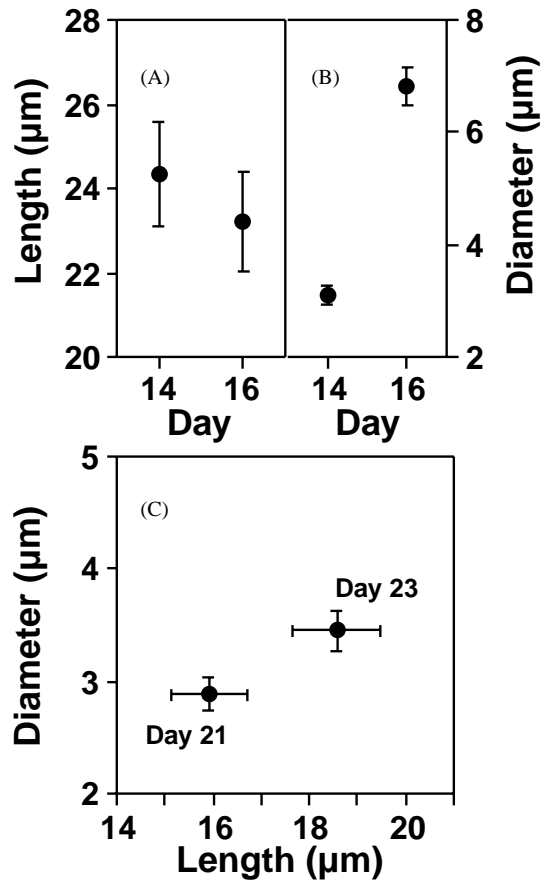

Fig. 8. Changes of size of most abundant diatom species in the mesocosm during days of maximum abundance (Days 14 and 21, of the first and second bloom, respectively) and after those days (Days 16 and 23). (A) Average length of *N. closterium*; (B) average diameter of *T. oceanica*; and (C) average length and diameter of *S. costatum*. Bars represent standard error ($18 < n < 190$). Characteristic dimensions were considered depending on the specie.

someter (Fig. 11A) show that beam attenuation peaks always preceded maxima of particles detected by IAS, suggesting a transfer of matter from smaller particles to larger ones.

TEP dynamics showed a pattern similar to that of bacterial abundance dynamics. The concentration of TEP increased exponentially to a maximum of about $1400 \, \mu g \, Xeq. \, l^{-1}$ after the first bloom and maintained high values until the end of the experiment (Fig. 12A). Identically, TEP expressed as number of particles stained with Alcian Blue per

liter maintained high values (around $3.5 \times 10^8 \, l^{-1}$) after the first phytoplankton maximum (Fig. 12B). Abundance of CSP was lower ($< 2 \times 10^8 \, l^{-1}$) and without a clear tendency during the experiment. During the first and second event of aggregation recorded by the IAS, TEP and CSP size spectra (Fig. 12C) had similar tendencies (but with significant different slopes), increasing their size as they aggregated. During the third aggregation event the proportion of larger sizes of TEP and CSP increased again after the chl *a* maximum and
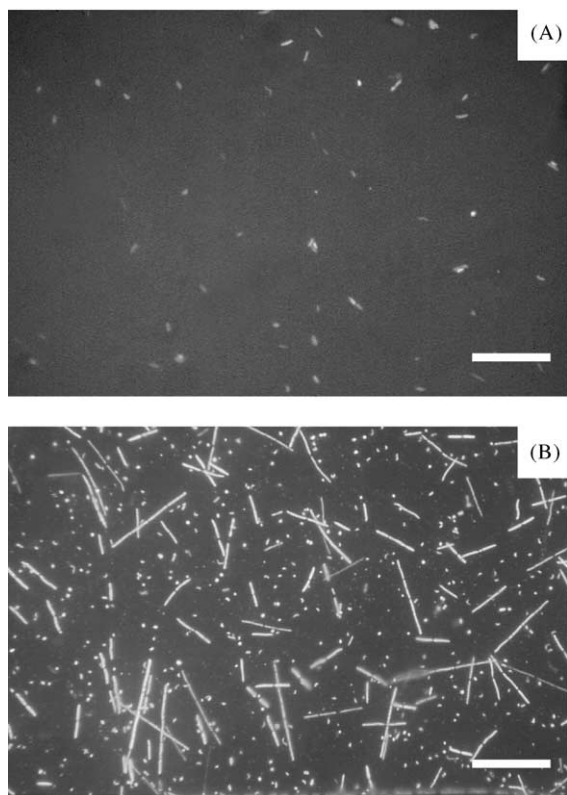
Fig. 9. Epifluorescence micrographs of DAPI-stained bacteria before and after the course of the blooms: (A) Day 0 and (B) Day 29. Scale bars are 10 μm long.

decreased when the aggregation abundance reached its maximum. As their abundance declined in the case of TEP this was probably due to the incorporation of exopolymers in aggregates that were out of the size range of microscopic analyses. This is not true for to CSP as their concentration rose on Day 23, a moment of increasing aggregate abundance.

4. Discussion

Both the high time resolution and wide size range records resolved particle size distribution dynamics during aggregation of sestonic material associated with diatom blooms. The volume concentration of aggregates ($mm^3 l^{-1}$) obtained by the IAS showed two peaks occurring with a time delay from 1 to 3 days after the peak concentration of the diatom blooms. This suggests that the process of aggregate formation from diatoms might have a time scale of the order of hours/days. This time scale for the transfer of matter from smaller to larger particles is also present in observations of the attenuation of a beam of 660 nm light, a signal usually associated with the concentration of small particles ($< 20 \, \mu m$, Chung et al., 1998). Beam attenuation peaks always preceded maxima of aggregate concentration by several hours. This lag ranged from 12 h for the first particle maximum Day 4, to 22 and 78 h for the peaks corresponding to the two diatom blooms.

Predictions done by Jackson (1990) using coagulation theory, where the greater increase in concentrations of larger particles occurred in half a day, agree with the time scales estimated empirically from the present set of data. Time scales similar to those recorded in this study can also be derived from aggregate records in the field. Monitoring by non-intrusive photography a diatom bloom in Bedford Basin, Krank and Milligan (1988) found that large flocs became visible 3 days after the bloom peaked. Also, high concentrations of marine snow aggregates have been observed to form within only a few days of a bloom peak (Logan et al., 1995). These field observations are affected by the difficulty of high temporal resolution sampling in natural systems. The battery of data from the present study permits us to determine the lowest resolution needed to achieve the same empirical result, which narrows previous theoretical scales. We observed that if only one size spectra had been registered each 2 h, the time scale for the aggregation process would have varied by only 1 h in the last aggregation maximum, and the magnitude would have decreased by only 3% (Table 2). However, if we decrease the sampling resolution to register only six size spectra each day, then the time scale would be misleading as it would be a 6 h difference between the aggregation event and the first diatom bloom. With this sampling resolution, the first particle maximum of Day 4 would decrease by 32%. Therefore, at least 12 spectra each day are
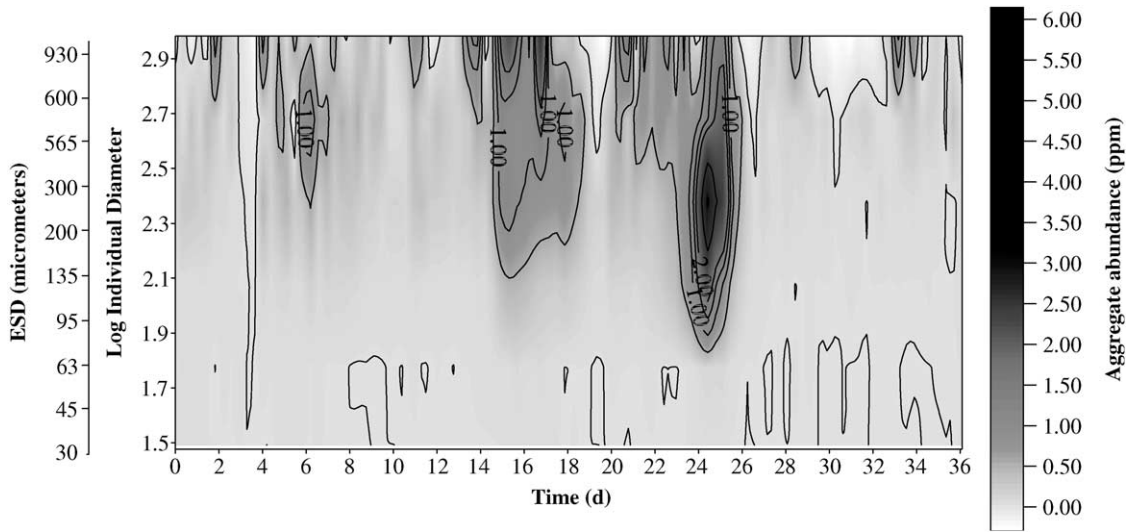
Fig. 10. Logarithmic size distribution of all particles in the mesocosm larger than 20 μm in diameter (ESD) during the experiment. Data are arranged into size classes of ESD (μm) whose amplitude is equal to the lower limit of that class (the first size class is 20–40 μm of ESD). Concentration is expressed as total particle volume (mm^3) per liter (ppm) in each size class.

Table 1
Average size (expressed as volume) ratios between individual particle types (TEP, CSP and plankton) and aggregates during the development of the aggregate maxima of Days 15–17 and 23–25

Day	Size ratio		
	TEP:aggregates	CSP:aggregates	Plankton:aggregates
15	0.06	0.08	
16	0.08	0.04	0.05
17	0.07	0.05	
23	0.06	0.05	0.07
25	0.05		

Plankton (both autotrophic and heterotrophic) was measured by light microscopy. No significant differences were found between size ratios of the two events.

needed to sample accurately any experiment aimed at studying aggregation of diatoms. The fact that our experimental design largely resolved this time scale gives solid support to this scale as the natural pace of the process and to the derivations obtained from the results achieved with this design.

Mesocosm experiments have been used as analogues of more complete, complex and difficult natural systems (Alldredge and Jackson, 1995; Kendrick et al., 1996; Pitta et al., 1997; Sanders and Purdie, 1998; Escaravage et al., 1999). A wide range of variables of interest can be measured and controlled within mesocosms. In the present study, a relevant variable in the process of coagulation, the turbulence, could be controlled. The turbulence levels used in experiments with plankton greatly exceed on average the range of the dissipation of turbulent energy usual for the ocean (Peters and Redondo, 1997). This methodological restriction is associated with the difficulty of generating low levels of turbulence (which usually implies substantial mass loss by sedimentation in closed environments) and keeping dynamic similarity with the ocean (Reynolds number must be similar to the natural system). The present mesocosm emulates physical conditions of an oceanic mixed layer (with dissipation turbulence energy on the order of $10^{-7} m^2 s^{-3}$), even though processes that in natural systems affect the size structure of the particles in the mesocosm have been eliminated. Natural advection, herbivorous grazing or vertical mixing, which can take the cells to zones where the irradiance is not sufficient for
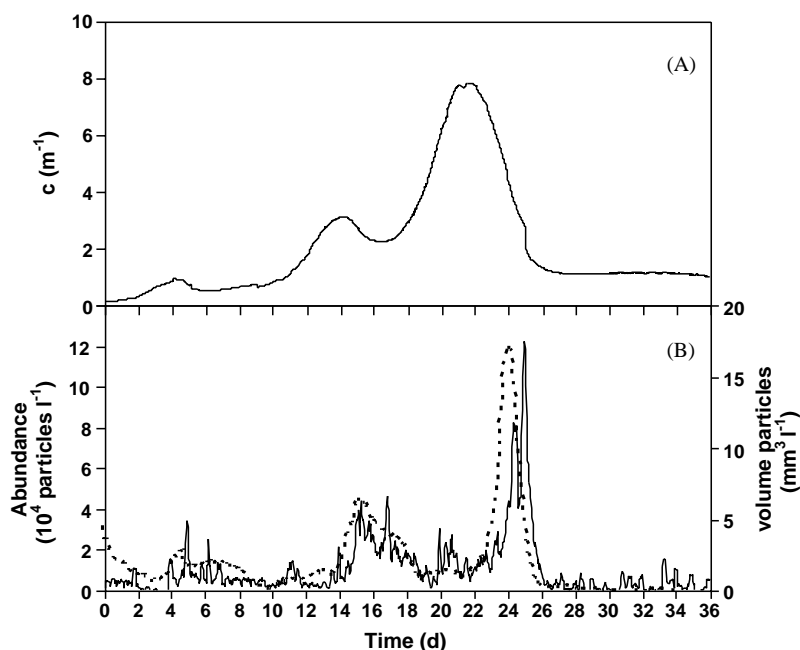
Fig. 11. Evolution of particle concentration over the course of the study. (A) Beam attenuation values (m^{-1}) measured with the transmissometer. (B) Total particle abundance (number l^{-1}), broken line, and total particle volume $(mm^3 l^{-1})$, solid line, measured with the non-intrusive image analysis system (IAS).

Table 2
Time lag (in hours) between beam attenuation maxima measured by the transmissometer and aggregate concentration maxima (expressed as ppm) registered by the IAS for different time resolutions

Frequency of sampling with IAS	Time lag (h)		
	1st Aggregation event (Day 4)	2nd Aggregation event (Day 15)	3rd Aggregation event (Day 24)
Each hour	19.44	21.77	78.86
Each 2 h	19.44 [0%]	21.77 [0%]	79.82 [3%]
Each 4 h	17.35 [32%]	27.77 [4%]	79.82 [3%]
Each 8 h	21.36 [53%]	27.77 [4%]	79.82 [3%]
Each 12 h	21.36 [53%]	19.85 [13%]	79.82 [3%]
Each 24 h	21.36 [53%]	19.85 [13%]	79.82 [3%]
Each 36 h	9.36 [83%]	19.85 [13%]	55.82 [64%]
Each 48 h	2.64 [71%]	43.85 [37%]	55.82 [64%]

Within brackets is the percent of decrease of the quantity of aggregate concentration maximum compared to the highest time resolution of the study (one size spectrum each hour).

phytoplankton to perform photosynthesis (Sver-drup, 1953), are some of those processes. Although the device generating turbulence was designed to inhibit particle sedimentation, the corners of the mesocosm acted as matter traps. Once a particle got into the influence of one of these sites, the turbulent environment could not return that particle into suspension (Ruiz et al., 2002). In
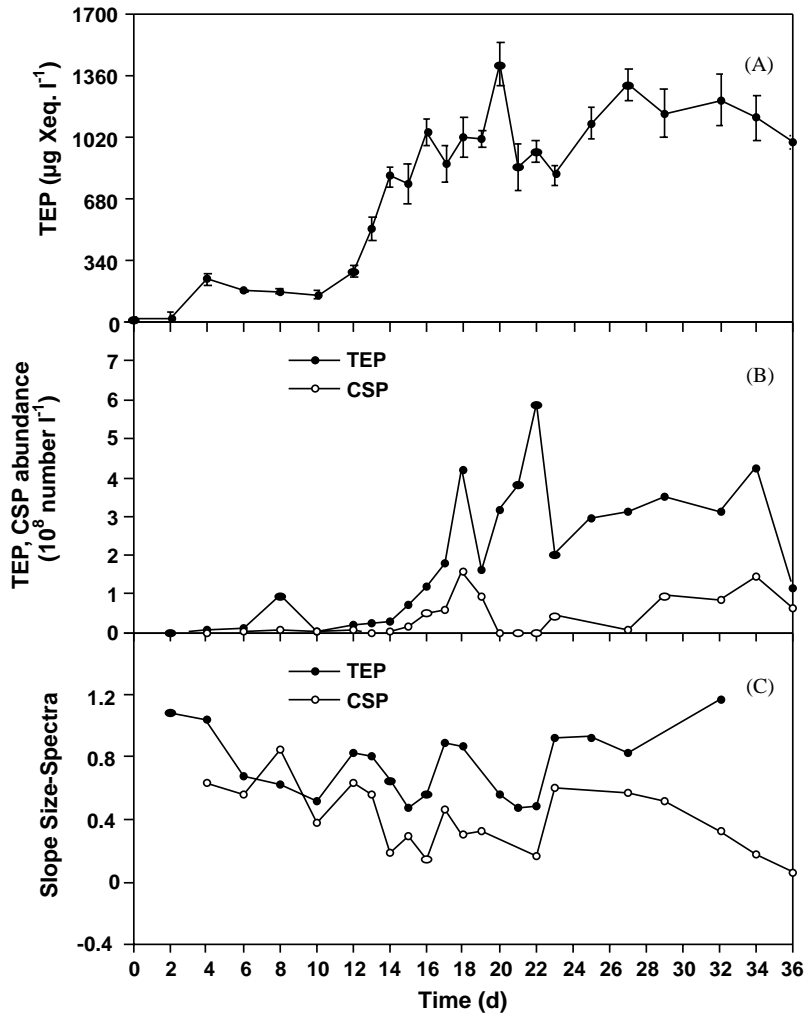
Fig. 12. (A) TEP concentration measured as μg of gum Xanthan equivalents (±SD, n = 5); (B) TEP and CSP abundance during the experiment; and (C) time evolution of slopes from TEP and CSP normalized volume size spectra.

consequence, material was lost in the mesocosm, and this was probably the final fate of the larger aggregates. Also, the presence of walls caused a high small-scale velocity shear that probably induced a break-up term higher than usual in the oceanic mixed layer affecting the concentration of larger aggregates and the maximum size reached as well.

Another feature of the experiment is related to nutrient. Initial nutrient concentrations were in the upper range of those found in field studies

(Riebesell, 1991b; Riebesell, 1992) to ensure the development of blooms, and the chl a maxima reached in the mesocosm was also high (Kepkay et al., 1997; Krank and Milligan, 1988). However, the formation of aggregates in this experiment agreed with that expected from the chlorophyll values reached and the relationship between chl a concentration of a phytoplankton bloom and the subsequent mass flocculation (Kepkay et al., 1993). During the first 10 days of the experiment, the nitrate reduction cannot be

explained just by phytoplankton consumption. From Day 1 to 4, the nitrate decreased 29% (a net reduction of 18 μM), while the chlorophyll was almost constant. In these first days, nitrate decline seem to be due to a partitioning between the other dissolved compartments (nitrite and ammonium) and, moreover, to an increase in the particulate compartment, also recorded by IAS system. From Day 4 to 10, the nitrate was reduced 4.6 μM (10%) and nitrite and ammonium increased 3.5 and 0.6 μM, respectively. During this period, PN in the water column decreased as a result of sedimentation of the first pulse of aggregates recorded on Day 4. This period was also characterized by an important increase in chlorophyll, and the ratio of chlorophyll and nitrate (not considering the one already transferred to the other dissolved compartments) is within the expected range.

The development of the microbial community is also affected in enclosure experiments (Ferguson et al., 1984; Jürgens et al., 2000). Changes in bacterial morphotypes have been observed in enclosures with marine waters (Shiah and Ducklow, 1995; Havskum and Hansen, 1997) and could result from differential grazing pressure by heterotrophic flagellates (Jürgens and Güde, 1994). In the present study, the high abundance of nanoflagellates after Day 16, with a maximum on Day 18, could explain the proliferation of filamentous bacteria toward the end of the experiment, as predation rates may have been lower for those bacteria. Although we did not differentiate between the trophic level (autotrophic or heterotrophic) of the nanoflagellates, we can estimate the maximum grazing rate in the mesocosm using the model developed by Peters (1994), which considers mean measured nanoflagellate size, bacterial and nanoflagellates concentrations and temperature. If all nanoflagellates were strictly bacterivorous, the maximum possible grazing rate would be 11 bact. $nanofl^{-1} h^{-1}$ on Days 14 and 16. Microbial interactions were probably affected by the artifacts of an enclosed experiment and the temperature of the study, but these estimated grazing rates were within the upper range of other studies (Zubkov and Sleigh, 1995) and confirmed that those interactions were nor-

mal. Also, the high concentrations of phaeopigments on those days fit with their generation by grazing of flagellates (Goldman and Caron, 1985). The C:N ratios reflected the healthy condition of cells in the mesocosm, and bacteria abundance were not outside the range observed in natural waters.

Notwithstanding inherent limitations of mesocosms, the development of two consecutive phytoplankton blooms is a common feature in natural systems that has been related to nutrient limitation (Tilman, 1977) and more recently to flocculation dynamics (Riebesell, 1991b; Crocker and Passow, 1995; Tiselius and Kuylenstierna, 1996; Kepkay et al., 1997). In our experiment, the demise of the first bloom (dominated by *N. closterium* and *T. oceanica*) was probably related to both processes since it occurred at limiting concentrations of P (Jørgensen et al., 1991), with N/P ratio (around 200) far away from the Redfield ratio of 16 and during high TEP production. Exudation of TEP per biomass increased as aggregation reached its maximum (Fig. 13C), whereas production of CSP did not show any relationship. High TEP production by *Nitzschia* spp. has also been observed during field studies (Logan et al., 1995) and it has been found that extracellular polysaccharide production was especially high in laboratory experiments when phosphate was limiting (Penna et al., 1999). Also, the autotrophic origin of TEP is clear from the significant positive correlations between TEP and chl *a* ($r = 0.93$) and from the phytoplankton microscopic observations during the development of this bloom where a thin layer stained with Alcian Blue was evident at the cell surface.

Aggregates observed after the first bloom (Fig. 5A) have an appearance similar to those of *N. angularis*, whose cells stick directly to each other when aggregating, thus generating dense flocs (Crocker and Passow, 1995). The differential aggregation was also reflected in the dynamics of these species' concentrations during the development of the first large aggregation maximum (Fig. 13A), when both *Nitzschia* and *Thalassiosira* decreased in number while *S. costatum* abundance kept increasing. During the development of this first aggregation event, significant positive correla-
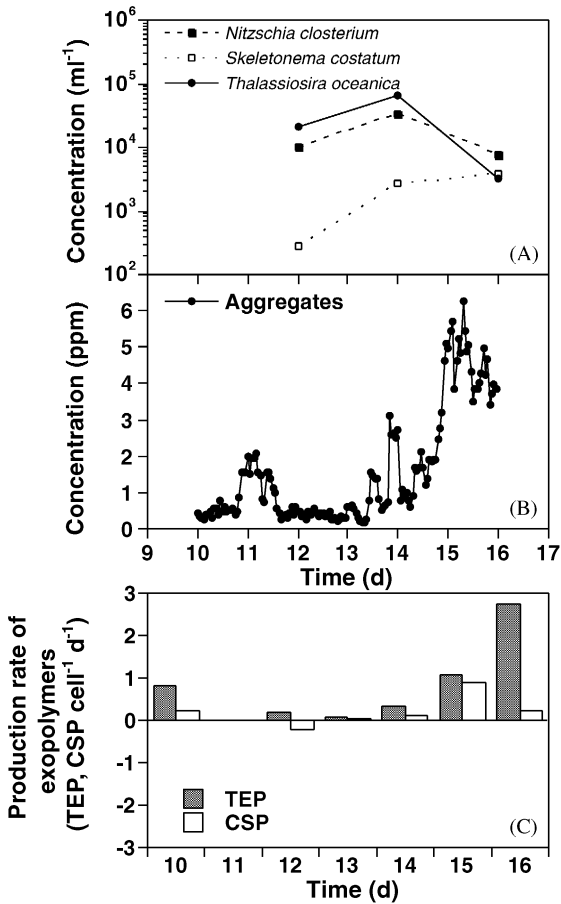
Fig. 13. Dynamics of diatom species, production of TEP and CSP per unit biomass during the development of the aggregate maximum after the first diatom bloom. (A) Diatom abundance (ml^{-1}), (B) aggregate concentration (ppm), and (C) production of TEP and CSP (exopolymer cell^{-1} d^{-1}). Phytoplankton measured by flow cytometry was used as biomass because both of the high correlation to microscopy phytoplankton data and the higher time resolution of flow cytometry data compared to microscopy.

Fig. 14. Similar to Fig. 13 but during the development of the aggregate maximum after the second diatom bloom.

tions were observed between TEP and total aggregate volume ($r = 0.82$), but this was not the case with the other exopolymer (CSP, $r = 0.65$), although the relation was positive too, showing a greater correlation between TEP dynamics and aggregate formation than with CSP.

The half saturation constant (K_s) for phosphate uptake by *Nitzschia* and *Thalassiosira* spp. is around 1 µM (Jørgensen et al., 1991), whereas by
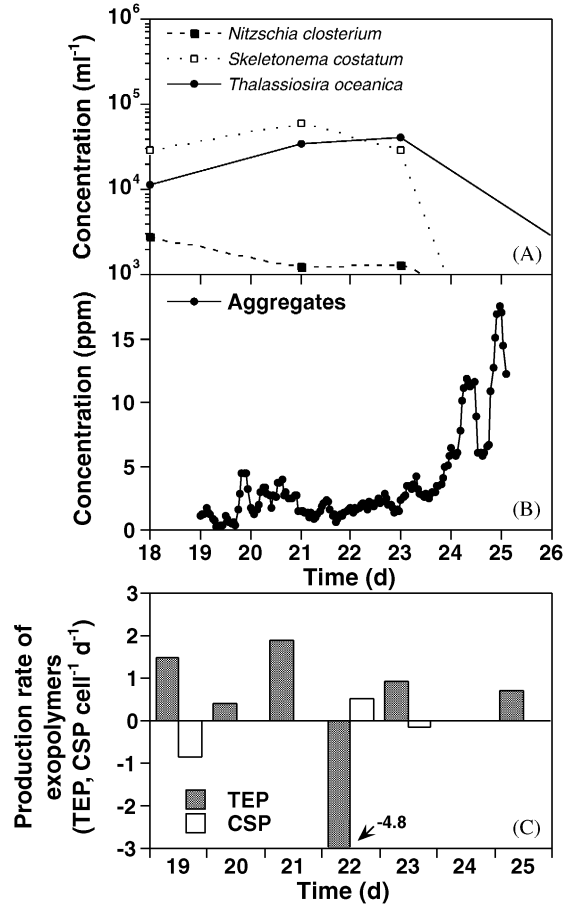
S. costatum it is two orders of magnitude lower (Tyrrel, 1999). This difference in phosphate affinity probably allowed *S. costatum* to outcompete the other two genera when phosphate concentrations were low. During the second bloom, silica may have limited growth as nitrate uptake should cease at silica concentrations below 2 µM (Dugdale and Wilkerson, 1998) and 0.8 µM is K_s for silicate uptake by *S. costatum* (Paasche, 1973). This second aggregation event was accompanied by the decrease of all diatom species (included *S. costatum*; Fig. 14A). At this moment, the proportion of TEP in total POC accounts for ≈35% (following the relation

between TEP volume and C content found by Mari, 1999), which is consistent with natural systems in which there is a prominent component of organic carbon in the photic zone (Alldredge et al., 1993; Passow et al., 1994; Schuster and Herndl, 1995).

Although TEP concentration during the second phytoplankton maximum maintained the high values reached during the first bloom, the production of TEP was lower (Fig. 14C) during the second bloom compared to the first bloom. During the development of the first bloom the average production of TEP normalized by standing stock was 38.9 TEP chl a^{-1}d^{-1}, whereas during the second bloom only 0.3 TEP chl a^{-1}d^{-1} was produced. Nearly, no production of CSP was registered during the development of this second bloom. No relationship was found between TEP and aggregate abundance during the development of the second large aggregate maximum (probably related to TEP accumulation in the water mentioned before), and CSP showed a negative correlation (although not significant) with aggregates ($r = -0.58$). Therefore, the role of CSP compared to TEP again appears to be less important in the flocculation events observed in the mesocosm as the second aggregation episode is the most intense. Nevertheless, phytoplankton and CSP distributions (Figs. 7, 8 and 12C) shifted toward greater sizes, and, as occurred with TEP, coincided with increasing aggregate total abundance and volume. As coagulation rates (and the subsequent export of carbon from the euphotic zone) depend both on particle spectra (abundance and size) and on stickiness, the number of theoretical collisions (which only considers the abundance and size of particles) can greatly differ from empirical results of aggregation because of the differences in the probability that particles remain attached after contact. Stickiness was not estimated and thus could not be used to confirm the role of CSP in aggregation. Nevertheless, a diagnosis based on data from this study showed that the potential sinking dynamics of POC could be estimated just from primary production (including nutrient limitation) and TEP together with particle and aggregate concentrations (Ruiz et al., 2002). The fact that this empirical model represented the process of aggregation without explicit consideration of CSP supports our conclusion of its lower significance. This difference in the role of TEP and CSP in aggregation, together with both the linking of aggregation and nutrient limitation to the phytoplankton succession and the narrowing of time scales for the transfer of mass from small to large particles, represents new insight concerning the aggregation process and the related vertical flux of carbon to the deep ocean. As these results were obtained from mesocosm experimentation, with its inherent limitations, further efforts must be made to extrapolate them to nature. Future studies to understand the mechanisms causing the lesser role of CSP in the formation of aggregates, in particular CSP stickiness, and the response of marine biota aggregation dynamics to changes in physical energy will provide us the means to estimate biological pump efficacy.

References

Alldredge, A.L., Gotschalk, C., 1989. Direct observations of the mass flocculation of diatom blooms: characteristics, settling velocities and formation of diatom aggregates. Deep-Sea Research I 36, 159–171.

Alldredge, A.L., Jackson, G.A., 1995. Aggregation in marine systems. Deep-Sea Research II 42, 1–9.

Alldredge, A.L., Passow, U., Logan, B.E., 1993. The abundance and significance of a class of large, transparent organic particles in the ocean. Deep-Sea Research I 40, 1131–1140.

Alldredge, A.L., Gotschalk, C., Passow, U., Riebesell, U., 1995. Mass aggregation of diatom blooms: insights from a mesocosm study. Deep-Sea Research II 42, 9–27.

Blanco, J.M., Echevarria, F., Garcia, C.M., 1994. Dealing with size-spectra: some conceptual and mathematical problems. Scientia Marina 58, 17–29.

Crocker, K.M., Passow, U., 1995. Differential aggregation of diatoms. Marine Ecology Progress Series 117, 249–257.

Chin, W.C, Orellana, M.V., Verdugo, P., 1998. Spontaneous assembly of marine dissolved organic matter into polymer gels. Nature 391, 568–572.

Chung, S.P, Gardner, W.D., Landry, M.R., Richardson, M.J., Walsh, I.D., 1998. Beam attenuation by microorganisms and detrital particles in the equatorial Pacific. Journal of Geophysical Research 103, 12669–12681.

Dam, H.G., Drapeau, D.T, 1995. Coagulation efficiency, organic-matter glues and the dynamics of particles during a phytoplankton bloom in a mesocosm study. Deep-Sea Research II 42, 111–123.

Dugdale, R.C., Wilkerson, F.P., 1998. Silicate regulation of new production in the equatorial Pacific upwelling. Nature 381, 270–273.

Eisma, D., Bale, A.J., Dearnaley, M.P., Fennessy, M.J., Van Leussen, W., Maldiney, M.-A., Pfeiffer, A., Wells, J.T., 1996. Intercomparison of *in situ* suspended matter (floc) size measurements. Journal of Sea Research 36, 3–14.

Escaravage, V., Prins, T.C., Nijdam, C., Smaal, A.C., Peeters, J.C.H., 1999. Response of phytoplankton to nitrogen input reduction in mesocosm experiments. Marine Ecology Progress Series 179, 187–199.

Ferguson, R.L., Buckley, E.N., Palumbo, A.V., 1984. Response of marine bacterioplankton to differential filtration and confinement. Applied Environmental Microbiology 47, 49–55.

Fowler, S.W., Knauer, G.A., 1986. Role of large particles in the transport of elements and organic compounds through the oceanic water column. Progress in Oceanography 16, 147–194.

Goldman, J.C., Caron, D.A., 1985. Experimental studies on an omnivorous microflagellate: implications for grazing and nutrient regeneration in the marine microbial food chain. Deep-Sea Research I 32, 899–915.

Havskum, H., Hansen, A.S., 1997. Importance of pigmented and colourless nano-sized protists as grazers on nano-plankton in a phosphate-depleted Norwegian fjord and in enclosures. Aquatic Microbial Ecology 12, 139–151.

Hill, P.S., Nowell, A.R.M., 1995. Comparison of two models of aggregation in continental-shelf bottom boundary layers. Journal of Geophysical Research 100, 22749–22763.

Jackson, G.A., 1990. A model of the formation of marine algal flocs by physical coagulation processes. Deep-Sea Research I 37, 1197–1211.

Jackson, G.A., 1995. Comparing observed changes in particle size spectra with those predicted using coagulation theory. Deep-Sea Research II 42, 159–184.

Jackson, G.A., Lochmann, S.E., 1992. Effect of coagulation on nutrient and light limitation of an algal bloom. Limnology and Oceanography 37, 77–89.

Jørgensen, S.E., Nielsen, S.N., Jørgensen, L.A., 1991. Handbook of Ecological Parameters and Ecotoxicology. Elsevier, Amsterdam, 1263pp.

Jürgens, K., Güde, H., 1994. The potential importance of grazing resistant bacteria in planktonic systems. Marine Ecology Progress Series 112, 169–188.

Jürgens, K., Gasol, J.M., Vaqué, D., 2000. Bacteria-flagellate coupling in microcosm experiments in the Central Atlantic Ocean. Journal of Experimental Marine Biology and Ecology 245, 127–147.

Kendrick, G.A., Jacoby, C.A., Heinemann, D., 1996. Benthic microalgae: comparison of chlorophyll a in a mesocosms and field sites. Hydrobiologia 326/327, 283–289.

Kepkay, P.E., Niven, S.E.H., Milligan, T.G., 1993. Low molecular weight and colloidal DOC production during a phytoplankton bloom. Marine Ecology Progress Series 100, 233–244.

Kepkay, P.E., Niven, S.E., Jellet, J.F., 1997. Colloidal organic carbon and phytoplankton speciation during a coastal bloom. Journal of Plankton Research 19, 369–389.

Kiørboe, T., Lundsgaard, C., Olensen, M., Hansen, J.L.S., 1994. Aggregation and sedimentation processes during a spring phytoplankton bloom: a field experiment to test coagulation theory. Journal of Marine Research 52, 297–323.

Krank, K., Milligan, T.G., 1988. Macroflocs from diatoms: in situ photography of particles in Bedford Basin, nova Scotia. Marine Ecology Progress Series 14, 183–189.

Lampitt, R.S., Hillier, W.R., Challenor, P.G., 1993. Seasonal and diel variations in the open ocean concentration of marine snow aggregates. Nature 326, 737–739.

Long, R.A, Azam, F., 1996. Abundant protein-containing particles in the sea. Aquatic Microbial Ecology 10, 213–221.

Logan, B.E., Grossart, H.P., Simon, M., 1994. Direct observation of phytoplankton, TEP and aggregates on polycarbonate filters using brightfield microscopy. Journal of Plankton Research 16, 1811–1815.

Logan, B.E., Passow, U., Alldredge, A.L., Grossart, H.P., Simon, M., 1995. Rapid formation and sedimentation of large aggregates is predictable from the coagulation rates (half-lives) of transparent exopolymeric particles (TEP). Deep-Sea Research II 42, 215–238.

Mari, X., 1999. Carbon content and C:N ratio of transparent exopolymeric particles (TEP) produced by bubbling exudates of diatoms. Marine Ecology Progress Series 183, 59–71.

McCave, I.N., 1984. Size spectra and aggregation of suspended particles in the deep ocean. Deep-Sea Research 31, 329–352.

Paasche, E., 1973. Silicon and the ecology of marine plankton diatoms. II. Silicate-uptake kinetics in five diatom species. Marine Biology 19, 262–269.

Parsons, T.R., Maita, Y., Lalli, C.M., 1984. A manual of chemical and biological methods for seawater analysis. Pergamon Press, Oxford, 173pp.

Passow, U., 2000. Formation of transparent exopolymer particles, TEP, from dissolved precursors. Marine Ecology Progress Series 192, 1–11.

Passow, U., Alldredge, A.L., 1994. Distribution, size and bacterial colonization of transparent exopolymer particles (TEP) in the ocean. Marine Ecology Progress Series 113, 185–198.

Passow, U., Alldredge, A.L., 1995. A dye-binding assay for the spectrophotometric measurement of transparent exopolymer particles (TEP). Limnology and Oceanography 40, 1326–1335.

Passow, U., Alldredge, A.L., Logan, B.E., 1994. The role of particulate carbohydrate exudates in the flocculation of diatom blooms. Deep-Sea Research I 41, 335–357.

Penna, A., Bertuli, S., Penna, N., Magnani, M., 1999. Influence of nutrient ratios on the in vitro extracellular polysaccharide production by marine diatoms from the Adriatic Sea. Journal of Plankton Research 21, 1681–1690.

Peters, F., 1994. Prediction of planktonic protistan grazing rates. Limnology and Oceanography 39, 195–206.

Peters, F., Redondo, J.M., 1997. Turbulence generation and measurement: application to studies on plankton. Scientia Marina 61, 205–228.

Pitta, P., Giannakourou, A., Divanach, P., Kentouri, M., 1997. Planktonic food web in marine mesocosms in the Eastern Mediterranean: bottom-up or bottom-down regulation? Hydrobiologia 363, 97–105.

Platt, T., Denman, K., 1977. Organization in the pelagic ecosystem. Helgoländer wissenschaftliche Meeresuntersuchungen 30, 575–581.

Platt, T., Denman, K., 1978. The structure of pelagic ecosystem. Rapp. P.-V. Reun. Cons. int. Explor. Mer. 173, 60–65.

Porter, K.G., Feig, Y.S., 1980. The use of DAPI for identifying and counting aquatic microflora. Limnology and Oceanography 25, 943–948.

Riebesell, U., 1991a. Particle aggregation during a diatom bloom. I. Physical aspects. Marine Ecology Progress Series 69, 273–280.

Riebesell, U., 1991b. Particle aggregation during a diatom bloom. II. Biological aspects. Marine Ecology Progress Series 69, 281–291.

Riebesell, U., 1992. The formation of large marine snow and its sustained residence in surface waters. Limnology and Oceanography 37, 63–76.

Riebesell, U., Wolf-Gladrow, D.A., 1992. The relationship between physical aggregation of phytoplankton and particle flux: a numerical model. Deep-Sea Research I 39, 1085–1102.

Robinson, D.G., Ehlers, U., Herken, R., Herrmann, B., Mayer, F., Shütmann, F.-W., 1987. Methods of preparation for electron microscopy. Springer, Berlin, 190pp.

Ruiz, J., 1996. The role of turbulence in the sedimentation loss of pelagic aggregates from the mixed layer. Journal of Marine Research 54, 385–406.

Ruiz, J., Prieto, L., Ortegón, F., 2002. Diatom aggregate formation and fluxes: a modelling analysis under different size-resolutions schemes and with empirically determined aggregation kernels. Deep-Sea Research I 49, 495–515.

Sanders, R., Purdie, D.A., 1998. Bacterial response to bloom dominated by diatoms and *Emiliania huxley* in nutrient-enriched mesocosms. Estuarine, Coastal and Shelf Science 46, 35–48.

Scharek, R., Tupas, L.M, Karl, D.M., 1999. Diatom fluxes to the deep sea in the oligotrophic North Pacific gyre at Station Aloha. Marine Ecology Progress Series 182, 55–67.

Schuster, S., Herndl, G.J., 1995. Formation and significance of transparent exopolymer particles in the northern Adriatic Sea. Marine Ecology Progress Series 124, 227–236.

Shiah, F.K., Ducklow, H.W., 1995. Regulation of bacterial abundance and production by substrate supply and bacterivory: a mesocosm study. Microbial Ecology 30, 239–255.

Smetacek, V.S., 1985. Role of sinking in diatom life-history cycles: ecological, evolutionary and geological significance. Marine Biology 84, 239–251.

Smith, D.C., Steward, G.F., Long, R.A., Azam, F., 1995. Bacterial mediation of carbon fluxes during a diatom bloom in a mesocosm. Deep-Sea Research II 42, 75–97.

Stemman, L., 1998. Analyse spatio-temporelle de la matiere particulaire déterminée par une nouvelle technique vidéo, en Méditerranée Nord-Occidentale. Ph.D. Thesis, University of Paris VI, 180pp.

Sverdrup, H.U., 1953. On conditions for the vernal blooming of phytoplankton. Journal du Conseil Permanent International pour l'Exploration de la Mer 18, 287–295.

Tennekes, H., Lumley, J.L., 1972. A First Course in Turbulence. The MIT Press, Cambridge, MA, 300pp.

Tilman, D., 1977. Resource competition between planktonic algae: an experimental and theoretical approach. Ecology 58, 338–348.

Tiselius, P.M., Kuylenstierna, M., 1996. Growth and decline of a diatom spring bloom: phytoplankton species composition, formation of marine snow and the role of heterotrophic dinoflagellates. Journal of Plankton Research 18, 133–155.

Tyrrel, T., 1999. The relative influences of nitrogen and phosphorous on oceanic primary production. Nature 400, 525–531.

Unesco, 1994. Protocols for the Joint Global Flux Study (JGOFS) Intergovernmental Oceanographic Commission (Scientific Committee on Oceanic Research). Manual and Guides, 29pp.

Utermöhl, H., 1958. Zur vervollkommung der quantitativen Phytoplankton Methodik. Mitteilungen Internationale Vereinigung fuer Theoretische und Angewandte Limnologie 9, 1–38.

Vaulot, D., Courties, C., Partensky, F., 1989. A simple method to preserve oceanic phytoplankton for flow cytometric analyses. Cytometry 10, 629–635.

Zhou, J., Mopper, K., Passow, U., 1998. The role of surface-active carbohydrates in the formation of transparent exopolymer particles by bubble adsorption of seawater. Limnology and Oceanography 43, 1860–1871.

Zubkov, M.V., Sleigh, M.A., 1995. Bacterivory by starved marine heterotrophic nanoflagellates of two species which feed differently, estimated by uptake of dual radio-active labelled bacteria. FEMS Microbiology Ecology 17, 57–66.